NUCL SCI TECH (2017) 28:74
DOI 10.1007/s41365-017-0227-6

Soft X-ray ptychography method at SSRF

Chun-Peng Wang[1,2] · Zi-Jian Xu[1] · Hai-Gang Liu[1] · Xulei Tao[1,2] · Ren-Zhong Tai[1]

Received: 26 August 2016 / Revised: 21 October 2016 / Accepted: 25 October 2016 / Published online: 28 April 2017

Abstract Ptychography is a diffraction-based X-ray microscopy technique in which an extended sample is scanned by a coherent beam with overlapped illuminated areas and complex transmission function of the sample is obtained by applying iterative phase retrieval algorithms to the diffraction patterns recorded at each scanned position. It permits quantitatively imaging of non-crystalline specimens at a resolution limited only by the X-ray wavelength and the maximal scattering angle detected. In this paper, the development of soft X-ray ptychography method at the BL08U1A beamline of Shanghai Synchrotron Radiation Facility is presented. The experimental setup, experimental parameters selection criteria, and post-experimental data analyzing procedures are presented in detail with a prospect of high-resolution image reconstruction in real time. The performance of this newly implemented method is demonstrated through the measurements of a resolution test pattern and two real samples: Pt–Co alloy nanoparticles and a breast cancer cell. The results indicate that strong scattering specimens can be reconstructed to sub-20 nm resolution, while a sub-25 nm resolution for biological specimens can be achieved.

Keywords Ptychography · Coherent diffraction imaging · X-ray microscopy · Phase retrieval

1 Introduction

Since its first demonstration in 1999 [1], the coherent diffraction imaging (CDI) method has drawn extensive research interest and leads to the development of specialized instruments at synchrotron radiation facilities [2–10], X-ray free-electron lasers [11–14], and tabletop soft X-ray laser sources [15–17]. As a novel and powerful X-ray microscopy technique, CDI can deliver 2D or 3D high spatial resolution images of non-crystalline specimens. Unlike forming images with optical elements in traditional microscopes, a far-field diffraction pattern is recorded at an oversampling level [18, 19] and a subsequent phase retrieval iterative calculation is applied to reconstruct the sample image in CDI. CDI overcomes shortcoming of traditional X-ray microscopy methods, where the resolution is limited by performance of the X-ray optical elements, while the spatial resolution of CDI is limited only by the X-ray wavelength and the maximal scattering angle detected.

As a newly emerging CDI method, ptychography (also called "scanning CDI" or "ptychographic CDI") reconstructs complex transmission function of the sample from the whole set of diffraction patterns recorded as the sample is scanned across by X-ray beams (a localized wave field, often referred as a "probe"). The areas illuminated by the probe at adjacent scan positions are physically overlapped. As a consequence, each given sample area contributes to a series

This work was supported by the National Natural Science Foundation of China (NSFC) (Grant Nos. 11225527, 11575283, 11505277) and the Ministry of Science and Technology of China (2012CB825705).

✉ Zi-Jian Xu
xuzijian@sinap.ac.cn

✉ Ren-Zhong Tai
tairenzhong@sinap.ac.cn

[1] Shanghai Institute of Applied Physics, Chinese Academy of Sciences, Shanghai 201800, China

[2] University of Chinese Academy of Sciences, Beijing 100049, China

of diffraction patterns recorded, providing a significant amount of data redundancy in the dataset. Due to such redundancy in the recorded dataset, it is possible to: retrieve the amplitude and phase of complex transmission function of the sample and the probe wave field simultaneously [20, 21]; obtain super-resolved sample image by extrapolating the diffraction patterns beyond the detector aperture [22]; recover experimental uncertainties such as probe position errors [23–25]; and reconstruct stationary mixed states in the probe radiation, the sample and the detector plane [26]. Therefore, various types of information can be obtained from ptychography, in which the most attention-getting ones are the amplitude and phase image of sample transmittance. The sample amplitude image reflects the absorption of X-ray by the sample, while the phase image reflects the phase-shift of the light wave passing through the sample. Ptychography also removes the restrictions of classical CDI, such as the necessity to prepare isolated specimens with lateral size much smaller than that of illumination spot, and permits high-resolution imaging of specimens with unlimited lateral extent. Ptychography also improves iterative convergence, avoids algorithm stagnation, and non-unique solutions, which often happen in classic CDI.

The experimental setup of soft X-ray ptychography [27–29] shares a number of similarities with scanning microscopy techniques, such as the scanning transmission X-ray microscopy (STXM) [30], in that a probe scans across the sample with the transmitted (or diffracted) wavefield intensities recorded. Therefore, ptychography is the most suitable CDI method for STXM beamlines. In this paper, the detailed information of the soft X-ray ptychography method developed at the STXM endstation of the BL08U1A beamline at Shanghai Synchrotron Radiation Facility (SSRF) is presented together with the results of demonstration experiment.

2 Experimental setup

SSRF operates at 3.5 GeV electron beam energy of the storage ring. The soft X-ray spectromicroscopy beamline provides photon beams of 250–2000 eV, covering the absorption edges of major elements (K-edge of C, N, O, F, Na, Mg, Al and Si, and L-edge of P, S, Cl, K, Ca, Fe, Cu and Zn) in biology, environmental science, materials science and other fields. The detailed information of the BL08U1A beamline layout including front-end, branches and experimental endstations can be found elsewhere [31–34]. The soft X-ray ptychography method was developed based on the STXM endstation of this beamline. By replacing just the photomultiplier tube (PMT) detector with a direct X-ray CCD detector, the STXM setup can be easily adapted for ptychography.

The experimental setup is shown in Fig. 1. A Φ200 μm FZP (Fresnel zone plate) having a Φ80 μm central stop and 30 nm outermost zone width (mounted on the ZP holder) in combination with a Φ70 μm order sorting aperture (OSA) is placed downstream of the X-ray exit window, allowing only the first-order focused X-ray through and blocking the direct X-ray beam and all higher-order contributions. The sample holder is mounted on a 2D piezostage with an interferometric feedback control and closed-loop operation allowing for long-term stability and high scan precision. The scanning positional accuracy is limited by stage vibration and the interferometer noise and is estimated at 1–8 nm (RMS). As the resolution of ptychographic imaging does not depend on the illumination spot size on sample, specimens can be placed out of FZP focus. For all the measurements described below, we place sample 51.4 μm downstream of the FZP focus. The diffraction patterns are recorded at far field using a 16-bit PI-MTE:2048B ultrahigh vacuum compatible soft X-ray CCD detector, which is placed 74 mm downstream of the sample holder. A square cone mask is placed in front of the CCD detector to prevent stray light from the laser interferometer. The CCD chip has a 2048 × 2048 imaging array with 13.5 μm × 13.5 μm pixel size. The experiments are performed at 1.33×10^{-3} Pa (10^{-5} Torr) in the STXM chamber, and the CCD chip temperature is −50 °C to reduce the thermal noise and minimize the dark current. A read-out time is 4.5 s/frame in diffraction data acquisition.

3 Criteria of selecting experimental parameters

Experimental parameters to guarantee high-quality diffraction patterns for subsequent image reconstructions are discussed in this section. Figure 2 shows schematically

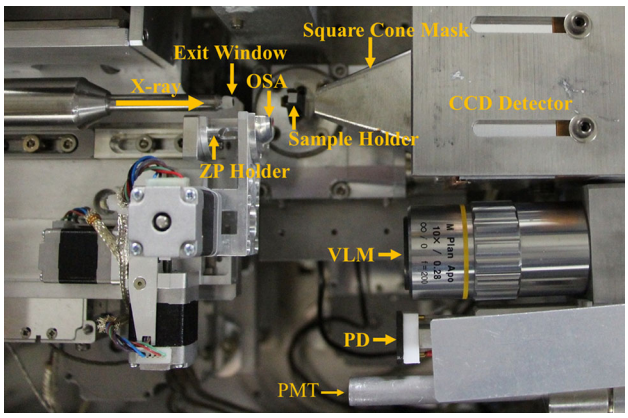

Fig. 1 The experimental setup for ptychography method in the STXM chamber. The FZP was mounted on the ZP holder. The visible light microscope (VLM), the photodiode (PD) and the PMT detector are out of the optical path during the experiments. (Color figure online)

the soft X-ray ptychography geometry with the key parameters.

We use the reconstruction algorithm based on discrete Fourier transform (DFT). It is valid only for diffraction patterns recorded in the far-field condition:

$$D_{\text{probe}}^2/(\lambda D_{\text{sd}}) << 1, \quad (1)$$

where D_{probe} is the diameter of the illumination spot (probe) on sample, λ is the wavelength, and D_{sd} is the sample–detector distance. When the sample is placed out of FZP focus and the offset distance is larger than the depth of FZP focus, the probe diameter (based on the geometry of the first-order focusing of FZP) can be calculated as:

$$D_{\text{probe}} = d_z D_{\text{zp}}/f, \quad (2)$$

where d_z is the offset distance of the sample from the FZP focal plane, D_{zp} is the FZP diameter, and f is its focal length. By tuning the defocus distance d_z, a probe of an arbitrary size can be obtained in a ptychography experiment. Note that if the sample is placed at the focal plane of the FZP, the effective probe size is usually 20% larger than the nominal outermost zone width [35].

The illumination probe overlapping ratio (Fig. 2) is defined as:

$$OR = 1 - \alpha/D_{\text{probe}}, \quad (3)$$

where a is the probe scanning step size. $OR \geq 60\%$ is necessary for confident image reconstruction [36, 37]. If the sample is at the focus of the FZP, ptychographic experiments should be conducted with a scanning step size that is comparable to the outermost zone width of the FZP. Using a defocus mode in the ptychography measurements allows for a larger scanning step size and can tolerate the machine instability in the data acquisition, but this mode results in a photon density decline in the illuminated area of the sample, and so does the intensity of diffraction signals and the signal-to-noise ratio, accordingly.

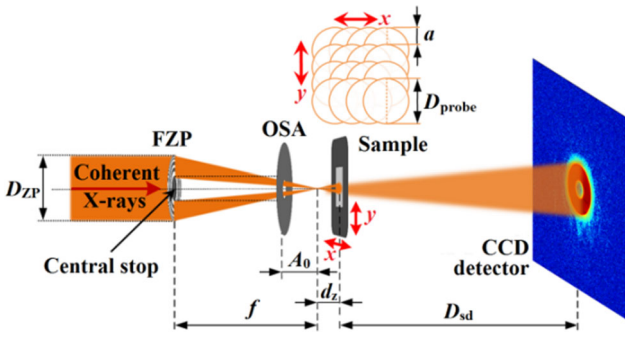

Fig. 2 Schematic layout of the soft X-ray ptychography with key parameters. The overlapped probe illuminated fields on sample is also shown. (Color figure online)

As shown in Fig. 3, once Eq. (1) is satisfied, if the sampling interval for an $N \times N$ array on the detector plane is Δ_{d} (i.e., the CCD pixel size), the pixel size Δ_{s} on the sample plane is determined by scaling of the discrete Fourier transform (DFT):

$$\Delta_{\text{s}} = \lambda D_{\text{sd}}/L_{\text{d}}, \quad (4)$$

where λ is the wavelength, D_{sd} is the propagation distance of the sample exit wave, and $L_{\text{d}} = N\Delta_{\text{d}}$ is the lateral width of the whole CCD chip. This relationship is extensively used throughout the image reconstruction process. The lateral size of the field of view on the sample plane for each scan position (the "CDI window") in a ptychography experiment is:

$$L_{\text{s}} = N\Delta_{\text{s}} = \lambda D_{\text{sd}}/\Delta_{\text{d}}. \quad (5)$$

To meet the oversampling requirements [18, 19] in the sample plane (real space), the probe size used in the experiment should be smaller than the CD window:

$$D_{\text{probe}} < L_{\text{s}}. \quad (6)$$

As the CDI window is determined by Eqs. (5), (6) is equivalent to the oversampling requirements on D_{sd} and Δ_{d} in the detector plane and is more convenient to use, especially when the sample is out of focus.

4 Data preprocessing and real-time image reconstruction

The recorded diffraction patterns must be properly processed before employing the iterative phase retrieval algorithms. The pre-reconstruction processing includes background noise removal, image cropping and binning.

As shown in Fig. 4, in order to remove the stray light scattering, CCD dark current, thermal or read-out noise and

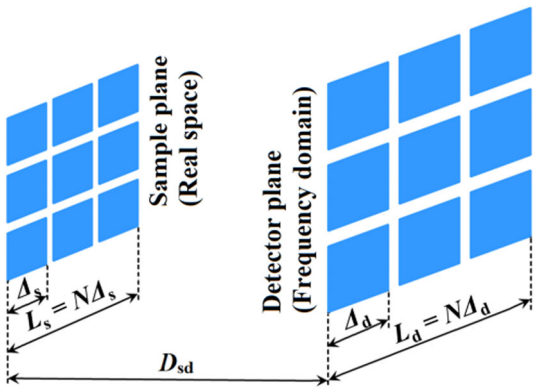

Fig. 3 Relationship between the sampling interval (i.e., pixel size) on the sample plane (real space) and that on the detector plane (frequency domain) which is determined by the scaling of the DFT. (Color figure online)

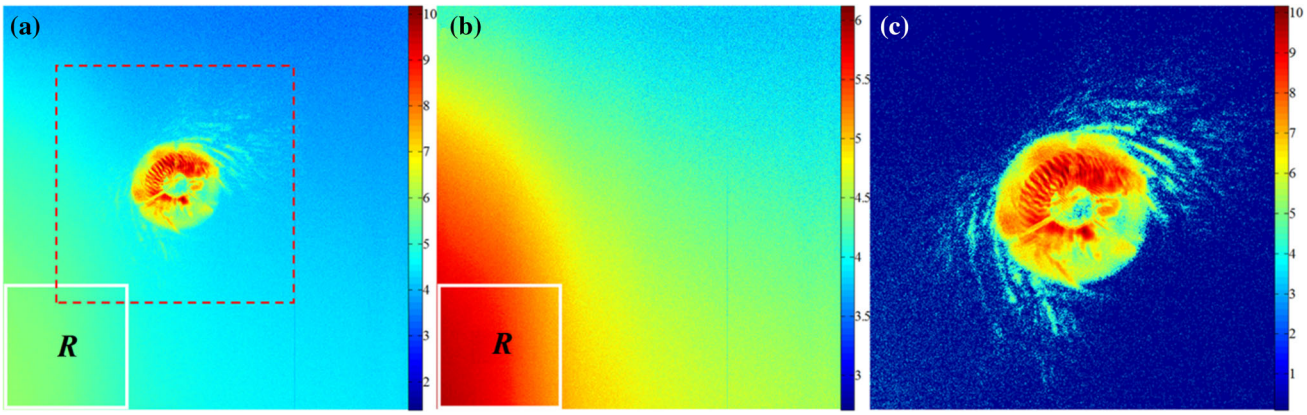

Fig. 4 Background noise removal and image cropping. (**a**) A typical raw diffraction pattern sized at 2048 × 2048 from the whole CCD chip. (**b**) The CCD dark image where the non-uniformly distributed background noise is clearly shown. (**c**) The diffraction pattern cut out from the *red dashed* 1200 × 1200 square area in (**a**) after employing the difference minimization noise removal method. The reference areas *R* used in the noise removal are also shown. All images are displayed in log-scale with *color scale bar* showing intensity counts. (Color figure online)

non-uniformities across the CCD chip, the pre-reconstruction processing begins with background noise removal. We use the difference minimization noise removal method, which is suitable for most ptychography datasets with clean diffraction patterns for image reconstruction. In this method, a reference area R in each diffraction pattern and in the CCD dark image is selected, in which the diffraction signals are negligible, and a rescaling factor α_i is calculated by minimizing the difference between the R areas using the least-squares method as follows:

$$\alpha_i = \frac{\sum_{x,y\in R} I_{\mathrm{M},i}(x,y) I_{\mathrm{D}}(x,y)}{\sum_{x,y\in R} I_{\mathrm{D}}^2(x,y)}, \tag{7}$$

where $I_{\mathrm{M},i}(x,y)$ is the measured intensity of the ith diffraction pattern and $I_{\mathrm{D}}(x,y)$ is the measured intensity of the CCD dark image. The effective diffraction patterns are then:

$$I_{\mathrm{eff},i} = I_{\mathrm{M},i}(x,y) - \alpha_i I_{\mathrm{D}}(x,y). \tag{8}$$

After background noise removal, the center of diffraction patterns is positioned and the diffraction patterns are cropped and binned. The binning operation is to take $m \times n$ pixels and average their intensity in a new pixel, which improves the signal-to-noise ratio of the recorded diffraction patterns.

The clean diffraction patterns are then used in the iterative phase retrieval computations to obtain the sample image and/or the probe image. We have implemented a number of iterative phase retrieval algorithms, including ptychographic iterative engine (PIE) [38], extended PIE (ePIE) and parallel PIE (pPIE) [21], position-correction PIE (pcPIE) [24], nonlinear optimization (NLO) [39], mixed-states PIE (msPIE) [26], up-sampling PIE (sPIE) [40], etc. Two HP-820z workstations are installed at the BL08U1A beamline for real-time image reconstructions. Each workstation has two Intel Xeon E5-2670 2.6 GHz CPUs (8 cores per CPU, 16 cores total) and 32 GB memory. One workstation has an NVIDIA GeForce GTX TITAN Z GPU card (stacked with 5760 CUDA cores and 12 GB on-board memory) and the other has an NVIDIA TESLA K40 GPU card (stacked with 2880 CUDA cores and 12 GB on-board memory). The reconstruction codes are built and run using MATLAB language. Making use of the MATLAB built-in functions that support CUDA GPU acceleration (such as fast Fourier transform), real-time reconstructions can be realized. For example, using a dataset including 100 diffraction patterns sized 1200 × 1200 (without binning), sample transmission and probe wave field can be reconstructed simultaneously with 300 ePIE iterations in 5 min using the workstation equipped with the TITAN Z card.

5 Results and discussion

We have imaged various samples using the ptychography method developed at the STXM beamline. In this section, we illustrate three typical examples: a Siemens star resolution test pattern, Pt–Co alloy nanoparticles, and a breast cancer cell.

5.1 Resolution test pattern

A Siemens star resolution test pattern (a lithographically fabricated star-shaped gold nanostructure deposited on a silicon nitride window) was measured by 708 eV X-rays, and the estimated probe size was ~3 μm. Using a 1200 × 1200 array of the CCD chip (diffraction patterns

were binned by 2 × 2 in reconstruction), the pixel size of the reconstructed image was 8.0 nm. A 10 × 10 raster grid of the sample positions was scanned with a 500 nm step size, and the exposure time at each position was 400 ms. Counting on the read-out time of CCD, it took about 8 min to acquire 100 diffraction patterns from a 7.5 μm × 7.5 μm square region of the test pattern.

To deal with the influence of finite spatial coherence within the probe radiation and to improve the reconstructed image quality, the mixed-states algorithm (multi-mode probes) was used [41]. The reconstructed amplitude and phase images of the test pattern are shown in Fig. 5a, b, respectively. The 30-nm spokes in the center area are clearly imaged in both images. However, in the phase image, phase wrapping occurs in the center area. Figure 5c shows the magnified version of the red dashed square part in Fig. 5a and is compared with the scanning electron microscope (SEM) image (Fig. 5d) and the STXM image (Fig. 5f, 15-nm scanning step) of the same area. The details in ptychography results are in agreement with the SEM image; particularly in the phase image, the phase wrapping areas are highly consistent with the contaminated areas in the SEM image. The STXM image quality is limited by the focus spot size of the FZP and has the worst image quality.

To quantitatively estimate the achieved spatial resolution, we made use of the azimuthal-averaged power spectral density (PSD) and the Fourier ring correlation (FRC) method. The PSD was obtained by averaging the squared modulus of the DFT of the image over all azimuths of the 2D DFT, and a multiplicative Kaiser–Bessel window function was applied prior to the DFT to minimize errors originating from truncations at the edges of the image [42]. The spatial resolution was determined by the critical frequency where the PSD curve significantly deviates from a power law decay into a regime dominated by random fluctuations (∼constant). The PSD curves of Fig. 5c, e are shown in Fig. 6a, b, respectively. The PSD-derived spatial resolution of the ptychography image is 8 nm (61.7 μm^{-1}), which is almost equal to the pixel size of the reconstructed image, whereas resolution of the STXM image is 32 nm (15.6 μm^{-1}). The FRC [43, 44] method was also used to evaluate the resolution of the ptychographic reconstructed image, by measuring the spatial frequency dependence of the cross-correlation of intensity of the Fourier transforms

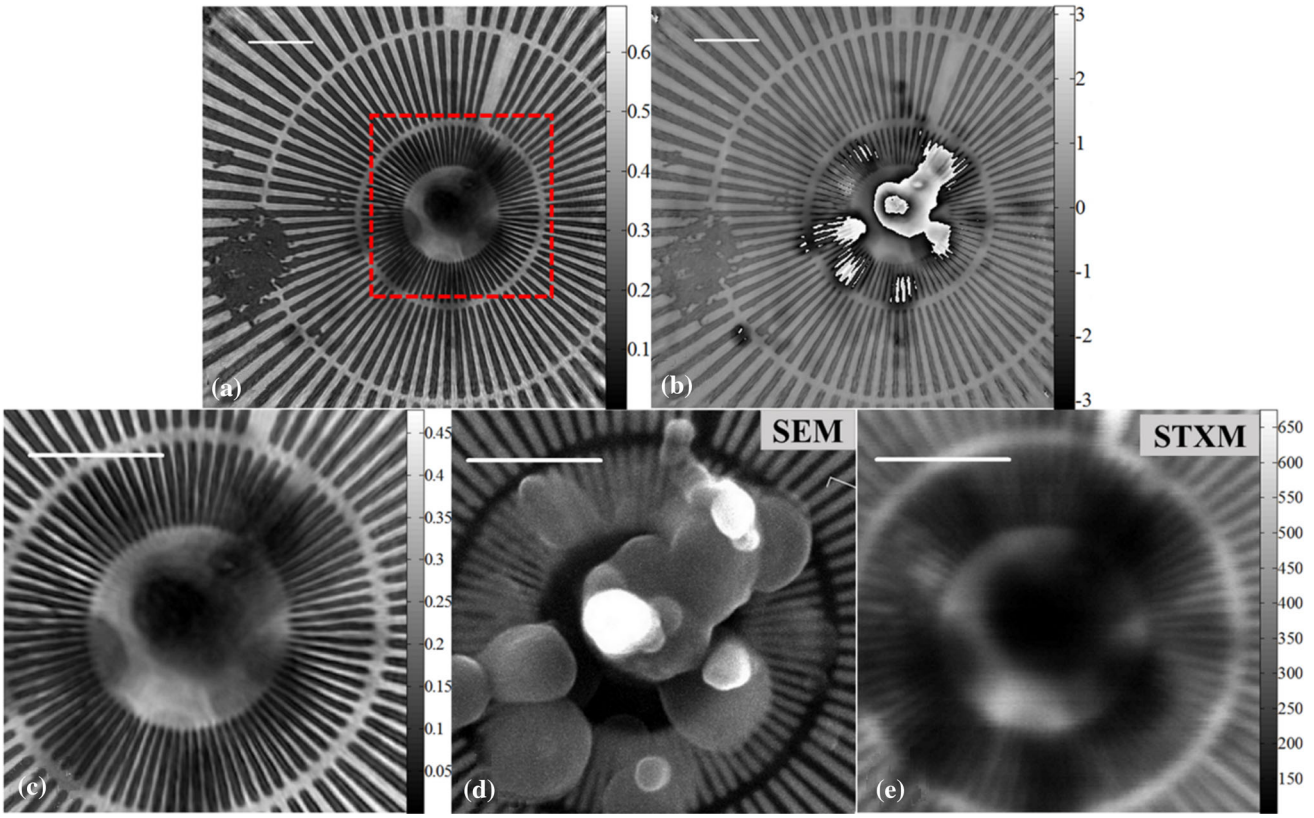

Fig. 5 Experimental results of the Siemens star resolution test pattern. *Scale bar* 1 μm. The reconstructed amplitude and phase images of the scanned area in ptychography are shown in (**a**) and (**b**), respectively. Phase wrapping can be seen in the *central area* of (**b**). (**c**–**f**) show images of the *red dashed squared area* in (**a**) obtained by (**c**) ptychography, (**d**) SEM and (**e**) STXM. The *gray scale bar* in amplitude images denotes the transmission ratio which is dimensionless and less than 1, while the unit of *gray scale bar* is radian in the phase image and photon count in the STXM image, respectively. (Color figure online)

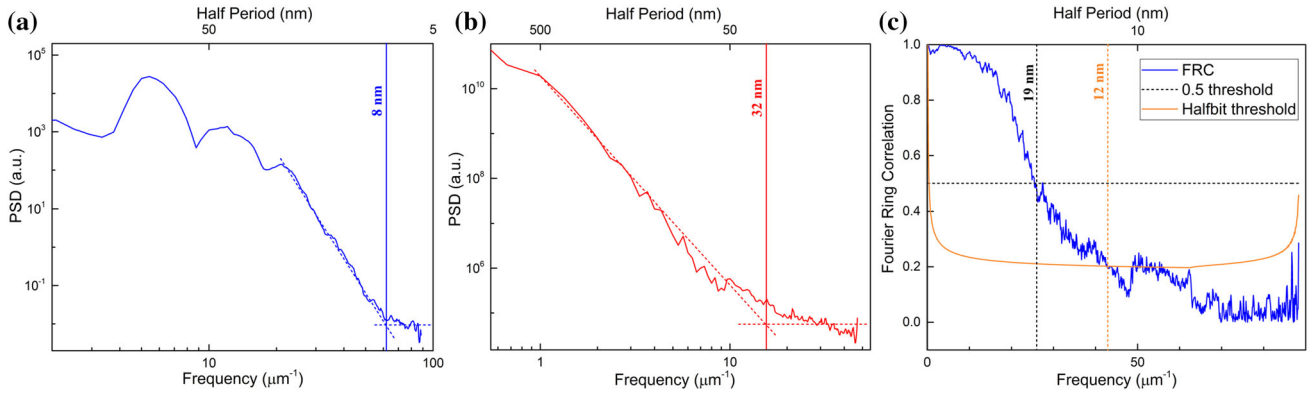

Fig. 6 Spatial resolution comparison of the ptychography method (**a**) and the STXM method (**b**) using PSD analysis. (**c**) The FRC resolution analysis of the ptychography reconstructions. The half-bit threshold determines the spatial resolution as 12 nm, and the 0.5 threshold determines the spatial resolution as 19 nm. (Color figure online)

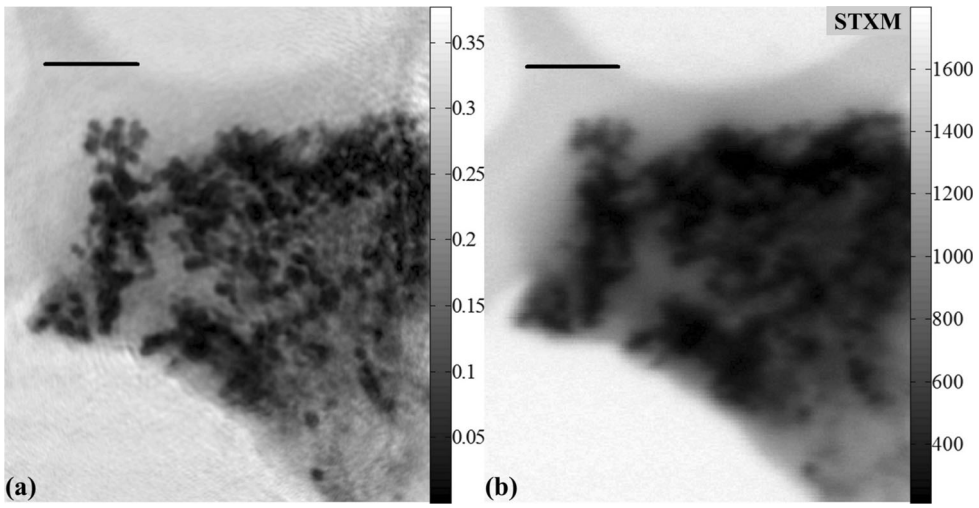

Fig. 7 Experimental results of the Pt–Co alloy nanoparticles. *Scale bar* 1 μm. (**a**) The reconstructed amplitude image of the scanned area using ptychography method. (**b**) The STXM image of the same area as (**a**) with 20-nm scanning steps. The *gray scale bar* in amplitude images denotes the transmission ratio which is dimensionless and less than 1, while the unit of *gray scale bar* is photon count in the STXM image

from two independent reconstructions under different initial conditions. The FRC result is shown in Fig. 6c, the spatial frequency where the FRC curve drops below the chosen threshold line is the estimated resolution. Two threshold lines are used here, the half-bit threshold determines the spatial resolution to be 12 nm (42.9 μm^{-1}), and the 0.5 threshold determines the spatial resolution to be 19 nm. Compared to the FRC method, the PSD method gives an overoptimistic resolution value. But the spatial resolution improvement by ptychography over STXM is clearly shown in the PSD analysis.

5.2 Pt–Co alloy nanoparticles

The sample of Pt–Co alloy nanoparticles (Φ100–200 nm) dispersed on the carbon film of a Cu mesh was measured by 710 eV X-rays, in the estimated probe size of ~3 μm. Using a 1754 × 1754 array of the CCD chip (diffraction patterns were binned by 2 × 2 in reconstruction), the pixel size of the reconstructed image was 5.5 nm. A 6 × 10 raster grid of the sample positions was scanned in 500-nm steps, and the exposure time at each position was 400 ms. Counting on the read-out time of CCD, it took about 5 min to obtain 60 diffraction patterns from a 5.5 μm × 7.5 μm rectangular region of the sample.

The reconstructed amplitude image of the sample using the msPIE algorithm is shown in Fig. 7a, and the STXM image of the same area in 20-nm scanning steps is shown in Fig. 7b. Image quality improvement of the ptychography method relative to the STXM method is clearly visible. Figure 8 shows the spatial resolution analyses using PSD and FRC methods. The PSD-based resolution of the ptychography reconstructed image is 11 nm (45.6 μm^{-1}) which is twice the pixel size of the reconstructed image, while the resolution of the STXM image is 39 nm (13.0 μm^{-1}). From the FRC analysis, the half-bit threshold determines a spatial resolution of 15 nm (34.2 μm^{-1}),

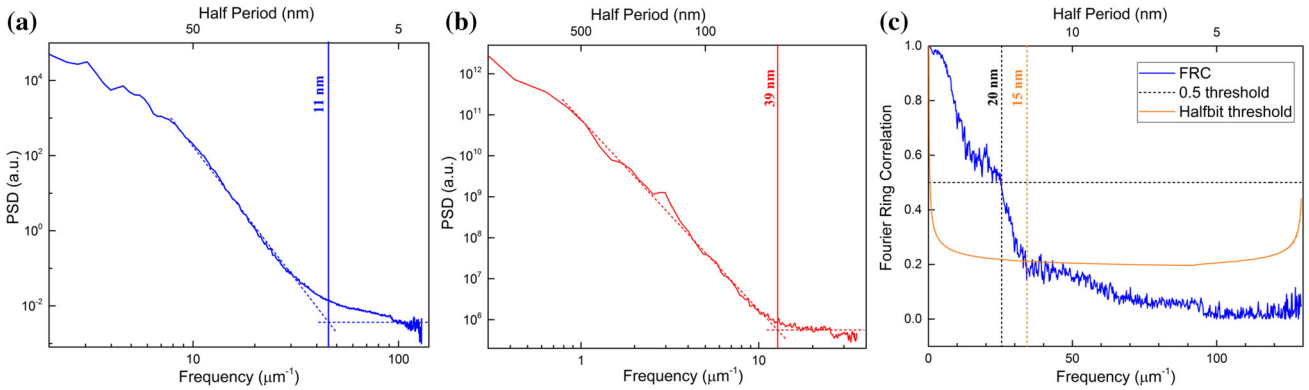

Fig. 8 Spatial resolution comparison of the ptychography method (**a**) and the STXM method (**b**) using PSD analysis. (**c**) The FRC resolution analysis of the ptychography reconstructions. The half-bit threshold determines the spatial resolution as 15 nm, and the 0.5 threshold determines the spatial resolution as 20 nm. (Color figure online)

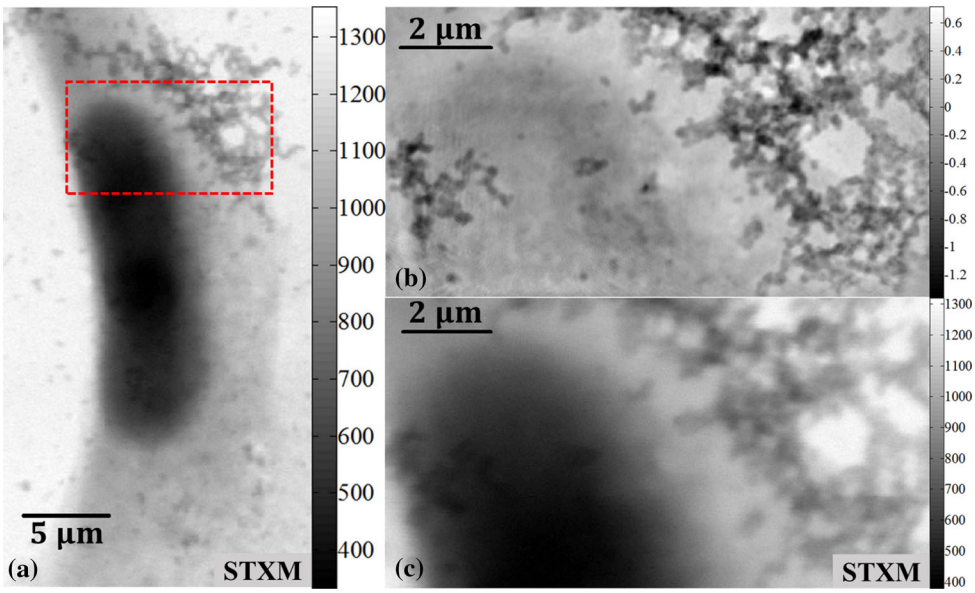

Fig. 9 Experimental results of the breast cancer cell. (**a**) An STXM image of one whole breast cancer cell with 100-nm scanning steps. *Scale bar* 5 μm. (**b**) The reconstructed phase image of the *red dashed rectangular area* in (**a**) using ptychography method. *Scale bar* 2 μm. (**c**) The STXM image of the same area as (**b**) with 30-nm scanning steps. *Scale bar* 2 μm. The unit of the *gray scale bar* is radian in the phase image and photon count in the STXM images, respectively. (Color figure online)

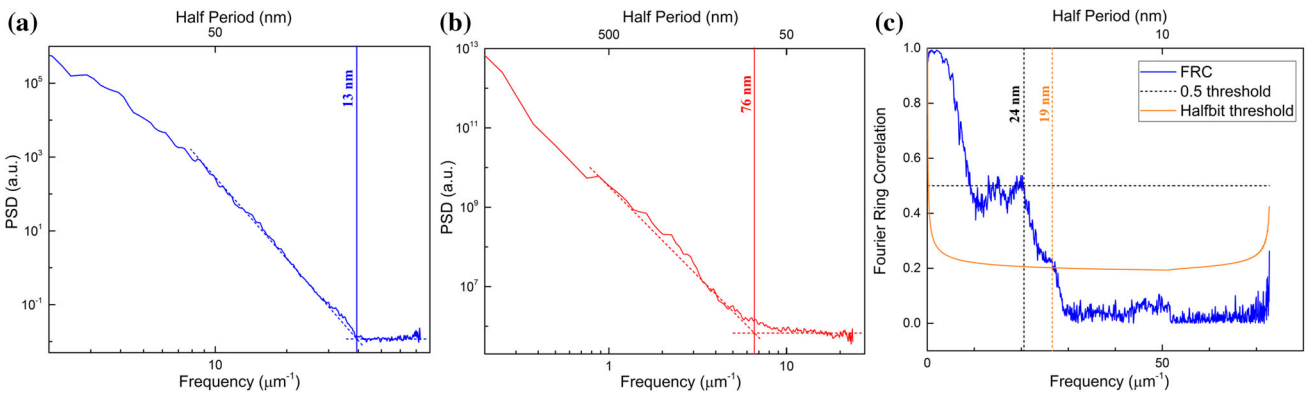

Fig. 10 Spatial resolution comparison of the ptychography method (**a**) and the STXM method (**b**) using PSD analysis. (**c**) The FRC resolution analysis of the ptychography reconstructions, the half-bit threshold determines the spatial resolution as 19 nm and the 0.5 threshold determines the spatial resolution as 24 nm. (Color figure online)

while the 0.5 threshold determines a spatial resolution of 20 nm (25.3 μm^{-1}).

5.3 Breast cancer cell

The breast cancer cells stained with ZnSe quantum dots were deposited on a silicon nitride window. An STXM image of a whole cell in 100-nm scanning steps is shown in Fig. 9a, obtained by 710 eV X-rays, in the estimated probe size of $\sim$3 μm. Using a 1024 × 1024 array of the CCD chip (without binning in reconstruction), the pixel size of the reconstructed image was 9.7 nm. A 16 × 9 raster grid of the sample positions was scanned in 700-nm steps, and the exposure time for each position was 600 ms. Counting on the read-out time of CCD, it took about 12 min to acquire the 144 diffraction patterns from a 13.5 μm × 7.9 μm rectangular region of the cell, which is shown in Fig. 9(a) with a red dashed rectangle.

The reconstructed phase image of the cell using ePIE algorithm is shown in Fig. 9b, and the STXM image of the same area in 30-nm scanning steps is shown in Fig. 9c. Image quality improvement of the ptychography method relative to the STXM image is clearly visible. The spatial resolution analysis using the PSD and FRC methods is shown in Fig. 10. The PSD-based resolution of the ptychography reconstructed image is 13 nm (39.4 μm^{-1}), while the resolution of the STXM image is 76 nm (6.6 μm^{-1}). From the FRC analysis, the half-bit threshold determines a spatial resolution of 19 nm (35.1 μm^{-1}) and the 0.5 threshold determines a spatial resolution of 24 nm (20.6 μm^{-1}).

The reconstructed images of the three examples above show great quality improvement compared with the STXM images. The performance of the soft X-ray ptychography method at BL08U1A beamline of SSRF is demonstrated by the three examples in this section, indicating a sub-20 nm resolution for strong scattering specimens and a sub-25 nm resolution for biological specimens.

6 Conclusion

Ptychography is a powerful X-ray microscopy technique for studying nanoscale specimens in biology, environmental science, materials science, and other fields. To improve the spatial resolution of the BL08U1A STXM beamline of SSRF, we have developed the soft X-ray ptychography method. The experimental setup and detailed procedures of the developed soft X-ray ptychography method are presented. The performance of this method is evaluated by imaging experiments of different kinds of samples in material science and life science. The spatial resolution achieved for strong scattering specimens is sub-20 nm. For biological specimens such as the breast cancer cells stained with ZnSe quantum dots, we have achieved a spatial resolution of sub-25 nm. The ptychography method at SSRF will be open to users soon and will be further improved to realize elements mapping by dual-energy and energy-stack ptychography. We hope the ptychography method can benefit users in various fields of science and technology.

References

1. J. Miao, P. Charalambous, J. Kirz et al., Extending the methodology of X-ray crystallography to allow imaging of micrometre-sized non-crystalline specimens. Nature **400**, 342 (1999). doi:10.1038/22498
2. J. Miao, T. Ishikawa, B. Johnson et al., High resolution 3D X-Ray diffraction microscopy. Phys. Rev. Lett. **89**, 088303 (2002). doi:10.1103/PhysRevLett.89.088303
3. D. Shapiro, P. Thibault, T. Beetz et al., Biological imaging by soft X-ray diffraction microscopy. Proc. Natl. Acad. Sci. U.S.A. **102**, 15343 (2005). doi:10.1073/pnas.0503305102
4. C.G. Schroer, P. Boye, J.M. Feldkamp et al., Coherent X-ray diffraction imaging with nanofocused illumination. Phys. Rev. Lett. **101**, 090801 (2008). doi:10.1103/PhysRevLett.101.090801
5. H. Jiang, D. Ramunno-Johnson, C. Song et al., Nanoscale imaging of mineral crystals inside biological composite materials using X-ray diffraction microscopy. Phys. Rev. Lett. **100**, 038103 (2008). doi:10.1103/PhysRevLett.100.038103
6. K.S. Raines, S. Salha, R.L. Sandberg et al., Three-dimensional structure determination from a single view. Nature **463**, 214 (2010). doi:10.1038/nature08705
7. J. Nelson, X. Huang, J. Steinbrener et al., High-resolution X-ray diffraction microscopy of specifically labeled yeast cells. Proc. Natl. Acad. Sci. U.S.A. **107**, 7235–7239 (2010). doi:10.1073/pnas.0910874107
8. H. Jiang, C. Song, C. Chen et al., Quantitative 3D imaging of whole, unstained cells by using X-ray diffraction microscopy. Proc. Natl. Acad. Sci. U.S.A. **107**, 11234 (2010). doi:10.1073/pnas.1000156107
9. B. Abbey, L.W. Whitehead, H.M. Quiney et al., Lensless imaging using broadband X-ray sources. Nat. Photonics **5**, 420 (2011). doi:10.1038/nphoton.2011.125
10. W. Yang, X. Huang, R. Harder et al., Coherent diffraction imaging of nanoscale strain evolution in a single crystal under high pressure. Nat. Commun. **4**, 1680 (2013). doi:10.1038/ncomms2661
11. H.N. Chapman, A. Barty, M.J. Bogan et al., Femtosecond diffractive imaging with a soft-X-ray free-electron laser. Nat. Phys. **2**, 839 (2006). doi:10.1038/nphys461
12. A.P. Mancuso, A. Schropp, B. Reime et al., Coherent-pulse 2D crystallography using a free-electron laser X-ray source. Phys. Rev. Lett. **102**, 035502 (2009). doi:10.1103/PhysRevLett.102.035502
13. M.M. Seibert, T. Ekeberg, F.R.N.C. Maia et al., Single mimivirus particles intercepted and imaged with an X-ray laser. Nature **470**, 78 (2011). doi:10.1038/nature09748
14. A.V. Martin, N.D. Loh, C.Y. Hampton et al., Femtosecond dark-field imaging with an X-ray free electron laser. Opt. Express **20**, 13501 (2012). doi:10.1364/OE.20.013501

15. R.L. Sandberg, A. Paul, D.A. Raymondson et al., Lensless diffractive imaging using tabletop coherent high-harmonic soft-X-ray beams. Phys. Rev. Lett. **99**, 098103 (2007). doi:10.1103/PhysRevLett.99.098103
16. R.L. Sandberg, C. Song, P.W. Wachulak et al., High numerical aperture tabletop soft x-ray diffraction microscopy with 70-nm resolution. Proc. Natl. Acad. Sci. U.S.A. **105**, 24 (2008). doi:10.1073/pnas.0710761105
17. A. Ravasio, D. Gauthier, F.R.N.C. Maia et al., Single-shot diffractive imaging with a table-top femtosecond soft X-ray laser-harmonics source. Phys. Rev. Lett. **103**, 028104 (2009). doi:10.1103/PhysRevLett.103.028104
18. J. Miao, J. Kirz, D. Sayre, The oversampling phasing method. Acta. Cryst. D **56**, 1312 (2000). doi:10.1107/S0907444900008970
19. J. Miao, T. Ishikawa, E.H. Anderson et al., Phase retrieval of diffraction patterns from noncrystalline samples using the oversampling method. Phys. Rev. B **67**, 174104 (2003). doi:10.1103/PhysRevB.67.174104
20. P. Thibault, M. Dierolf, A. Menzel et al., High-resolution scanning X-ray diffraction microscopy. Science **321**, 379 (2008). doi:10.1126/science.1158573
21. A.M. Maiden, J.M. Rodenburg, An improved ptychographical phase retrieval algorithm for diffractive imaging. Ultramicroscopy **109**, 1256 (2009). doi:10.1016/j.ultramic.2009.05.012
22. A.M. Maiden, M.J. Humphry, F. Zhang et al., Superresolution imaging via ptychography. J. Opt. Soc. Am. A **28**, 604 (2011). doi:10.1364/JOSAA.28.000604
23. A. Shenfield, J.M. Rodenburg, Evolutionary determination of experimental parameters for ptychographical imaging. J. Appl. Phys. **109**, 124510 (2011). doi:10.1063/1.3600235
24. A.M. Maiden, M.J. Humphry, M.C. Sarahan et al., An annealing algorithm to correct positioning errors in ptychography. Ultramicroscopy **120**, 64 (2012). doi:10.1016/j.ultramic.2012.06.001
25. F. Zhang, I. Peterson, J. Vila-Comamala et al., Translation position determination in ptychographic coherent diffraction imaging. Opt. Express **21**, 13592 (2013). doi:10.1364/OE.21.013592
26. P. Thibault, A. Menzel, Reconstructing state mixtures from diffraction measurements. Nature **494**, 68 (2013). doi:10.1038/nature11806
27. M. Beckers, T. Senkbeil, T. Gorniak et al., Chemical contrast in soft X-ray ptychography. Phys. Rev. Lett. **107**, 208101 (2011). doi:10.1103/PhysRevLett.107.208101
28. A.M. Maiden, G.R. Morrison, B. Kaulich et al., Soft X-ray spectromicroscopy using ptychography with randomly phased illumination. Nat. Commun. **4**, 1669 (2013). doi:10.1038/ncomms2640
29. D.A. Shapiro, Y.-S. Yu, T. Tyliszczak et al., Chemical composition mapping with nanometre resolution by soft X-ray microscopy. Nat. Photonics **8**, 765–769 (2014). doi:10.1038/nphoton.2014.207
30. P. Horowitz, J.A. Howell, A scanning X-ray microscope using synchrotron radiation. Science **178**, 608 (1972). doi:10.1126/science.178.4061.608
31. C. Xue, Y. Wang, Z. Guo et al., High-performance soft X-ray spectromicroscopy beamline at SSRF. Rev. Sci. Instrum. **81**, 103502 (2010). doi:10.1063/1.3491837
32. X. Zhang, Z. Xu, R. Tai et al., Ratio-contrast imaging of dual-energy absorption for element mapping with a scanning transmission X-ray microscope. J. Synchrotron Radiat. **17**, 804 (2010). doi:10.1107/S0909049510031250
33. S.M. Yang, L.S. Wang, J. Zhao et al., Developments at SSRF in soft X-ray interference lithography. Nucl. Sci. Tech. **26**, 010101 (2015). doi:10.13538/j.1001-8042/nst.26.010101
34. L.J. Zhang, Z.J. Xu, X.Z. Zhang et al., Latest advances in soft X-ray spectromicroscopy at SSRF. Nucl. Sci. Tech. **26**, 040101 (2015). doi:10.13538/j.1001-8042/nst.26.040101
35. D. Attwood, *Soft X-rays and extreme ultraviolet radiation: principles and applications* (Cambridge University Press, Cambridge, 2007)
36. O. Bunk, M. Dierolf, S. Kynde et al., Influence of the overlap parameter on the convergence of the ptychographical iterative engine. Ultramicroscopy **108**, 481 (2008). doi:10.1016/j.ultramic.2007.08.003
37. H.G. Liu, Z.J. Xu, X.Z. Zhang et al., Effects of missing low-frequency information on ptychographic and plane-wave coherent diffraction imaging. Appl. Opt. **52**, 2416 (2013). doi:10.1364/AO.52.002416
38. J.M. Rodenburg, H.M.L. Faulkner, A phase retrieval algorithm for shifting illumination. Appl. Phys. Lett. **85**, 4795 (2004). doi:10.1063/1.1823034
39. M. Guizar-Sicairos, J.R. Fienup, Phase retrieval with transverse translation diversity: a nonlinear optimization approach. Opt. Express **16**, 7264 (2008). doi:10.1364/OE.16.007264
40. D.J. Batey, T.B. Edo, C. Rau et al., Reciprocal-space up-sampling from real-space oversampling in X-ray ptychography. Phys. Rev. A **89**, 043812 (2014). doi:10.1103/PhysRevA.89.043812
41. C.P. Wang, Z.J. Xu, X.L. Tao et al., Improving the reconstructed image quality in ptychography using mixed states decomposition iterative phase retrieval algorithms. Nucl. Tech. **39**, 110102 (2016). doi:10.11889/j.0253-3219.2016.hjs.39.110102
42. R.N. Wilke, M. Priebe, M. Bartels et al., Hard X-ray imaging of bacterial cells: nano-diffraction and ptychographic reconstruction. Opt. Express **20**, 19232 (2012). doi:10.1364/OE.20.019232
43. R.P.J. Nieuwenhuizen, K.A. Lidke, M. Bates et al., Measuring image resolution in optical nanoscopy. Nat. Methods **10**, 557–562 (2013). doi:10.1038/nmeth.2448
44. M. Van Heel, M. Schatz, Fourier shell correlation threshold criteria. J. Struct. Biol. **151**, 250–262 (2005). doi:10.1016/j.jsb.2005.05.009